

We are IntechOpen, the world's leading publisher of Open Access books Built by scientists, for scientists

6,900

Open access books available

186,000

International authors and editors

200M

Downloads

Our authors are among the

154

Countries delivered to

TOP 1%

most cited scientists

12.2%

Contributors from top 500 universities



WEB OF SCIENCE™

Selection of our books indexed in the Book Citation Index
in Web of Science™ Core Collection (BKCI)

Interested in publishing with us?
Contact book.department@intechopen.com

Numbers displayed above are based on latest data collected.
For more information visit www.intechopen.com



Piezoelectric thin film deposition: novel self-assembled island structures and low temperature processes on silicon

Sharath Sriram, Madhu Bhaskaran and Arnan Mitchell
*Microplatforms Research Group, RMIT University
Australia*

1. Introduction

Lead zirconate titanate $\text{Pb}(\text{Zr}_{1-y}\text{Ti}_y)\text{O}_3$ is a material that is known for its high piezoelectric and ferroelectric properties. Thick and thin films of lead zirconate titanate (PZT) have been repeatedly used in a variety of piezoelectricity or piezoresistivity based sensors such as bio-sensing cantilevers (Park et al., 2005a) and pressure sensors (Maluf & Williams, 2004). PZT is one of many ceramic compounds with a general ABO_3 representation. Zirconium (Zr) and titanium (Ti) are B-site dopants of the compound and the ratio of Zr/Ti can alter the film properties such as the dielectric tunability (Yu et al., 2004). Certain A-site dopants (in place of a fraction of the lead atoms present in A-site locations) have been found to increase certain properties and introduce other properties. Examples of these are (i) lanthanum-doped PZT (PLZT) is known for enhanced electro-optic behaviour (Tunaboylu et al., 1998); (ii) stannum-doped PZT and niobium-doped PZT (PNZT) are known to exhibit shape memory behaviour, a property not exhibited by PZT (Yu & Singh, 2000); and (iii) the compound of interest in this chapter strontium-doped PZT (PSZT) has been reported to have improved piezoelectric, ferroelectric, dielectric tunability, and pyroelectric (infra-red radiation sensors by thermal effects) behaviour (Bedoya et al., 2000; Zheng et al., 2002; Araujo & Eiras, 2003; Yu et al., 2004).

Published literature on studies of PSZT material focuses on pellets and powders (Bedoya et al., 2000; Yu et al., 2004). However, the general consensus is that PZT and other doped-PZT compounds (e.g. PLZT and PNZT) can be deposited as thick or thin films under similar conditions, whether by sputtering or sol-gel techniques, as the percentage concentration of A-site dopants is generally very small. To exhibit piezoelectricity, ferroelectricity, and other properties the films need to be crystalline and not amorphous. The desirable crystalline phases of these films, termed perovskite, are generally rhombohedral or tetragonal (Randall et al., 1998; Yu et al., 2004).

RF magnetron sputter deposition of thin films of PZT and its doped variations (such as PLZT) have been reported in published literature (Kim et al., 1999; Wasa et al., 2004). Most published literature report deposition at temperatures of 500 °C to 700 °C (Kim et al., 1999; Wasa et al., 2004), followed in many cases by annealing at temperatures between 1000-1300 °C (Wasa et al., 2004). Such high temperature processing is undesirable when

working with metal, oxide, and nitride films on silicon, which is typically the case with most microsystem devices. This increases thermal stress between layers and can deform microstructures such as cantilevers, bridges, and membranes. Reports in published literature also discuss the difficulty in controlling orientation by sputtering (Park et al., 2005b).

This chapter reports on novel synthesis techniques for the deposition of piezoelectric thin films on to silicon substrates, which allows the use of microfabrication in the realisation of sensors, actuators, and transducers. It demonstrates an intermetallic reaction driven self-assembly process for formation of islands of piezoelectric and the use of lattice guiding by a metal layer to perform low temperature deposition of piezoelectric thin films. These coatings have been characterised extensively by spectroscopy and high resolution electron microscopy. For the first case, PSZT thin films were deposited on platinum (Pt) coated silicon substrates as platinum has been the conventional choice for deposition of PZT compounds. Utilising intermetallic reactions on silicon, preferential deposition sites were defined for island-structured deposition for optical sensing. The second case focussed on the challenge of low temperature crystallization of complex oxide thin films. Deposition of such materials is often carried out at elevated temperatures in excess of 600 °C. This chapter demonstrates one of the first instances of deposition of preferentially oriented strontium-doped lead zirconate titanate thin films at a relatively low temperature of 300 °C. This was achieved by carrying out deposition on gold-coated silicon substrates which exert a guiding influence on thin film growth due to similarity in lattice parameters.

2. Experimental Details

2.1 Bottom electrode deposition

Silicon (100) substrates were dipped in hydrofluoric acid to remove the native oxide layer. The desired bottom electrode configuration was deposited by electron beam evaporation (at room temperature and under vacuum of 1×10^{-7} Torr). The four bottom electrode configurations used for this study were (i) platinum thin films with titanium adhesion layer (Pt 200 nm on Ti 20 nm on Si), (ii) platinum thin films with titanium dioxide adhesion layer (Pt 200 nm on TiO₂ 20 nm on Si), (iii) gold thin films with titanium adhesion layer (Au 150 nm on Ti 15 nm on Si), and (iv) gold thin films with titanium adhesion layer and a silicon dioxide intermediate layer (Au 150 nm on Ti 15 nm on SiO₂ 200 nm on Si). All bottom electrode layers for each type of sample were sequentially deposited without breaking vacuum.

2.2 Thin film deposition

Thin films of strontium-doped lead zirconate titanate (PSZT) of composition $(\text{Pb}_{0.92}\text{Sr}_{0.08})(\text{Zr}_{0.65}\text{Ti}_{0.35})\text{O}_3$ (700 nm or 1.6 μm thick) were deposited on metal coated silicon substrates by RF magnetron sputtering in a 10% oxygen balance argon atmosphere at a pressure of 10 mTorr (Sriram et al., 2009a) from a 100 mm diameter target of composition $(\text{Pb}_{0.92}\text{Sr}_{0.08})(\text{Zr}_{0.65}\text{Ti}_{0.35})\text{O}_3$. A 3-inch resistive substrate heater was used, which was compatible with deposition in an oxygen atmosphere, and samples were placed in direct contact with the heater. Very accurate control of temperature was achieved using a Model 808 temperature controller programmer (Eurotherm Controls, Inc.). The post-deposition cooling rate was found to influence the degree of perovskite orientation in the thin films (Sriram et al., 2006a) and so, a cooling rate of 5 °C/min was chosen.

2.3 Transmission electron microscopy (TEM) analysis

The transmission electron microscopy (TEM) analysis was carried out at an accelerating voltage of 200 kV on a JEOL 2010F TEM equipped with a Gatan Imaging Filter (GIF2001) and an EmiSpec E Vision energy dispersive X-ray analysis (EDX) system. Plan view specimens for *in situ* TEM analysis were prepared by mechanically grinding away the backing silicon from the film, with the aid of a calibrated disc grinder. The specimens were then ion milled to electron transparency at room temperature using 4 kV argon ions incident at 5°, with dual beam milling from the back surface of the specimen. A TEM holder with a programmable heating element, and temperature accuracy of ± 0.5 °C, was used. Cross-sectional TEM specimens were prepared by gluing coated samples face-to-face with backing silicon, using high strength epoxy resin. A core (2.3 mm in diameter) was then ultrasonically machined with the interface of interest at the centre of the core. The core was then glued into a brass tube of 3 mm external diameter. This was then sawed into 500 μm thick sections, ground, and ion milled (Ar^+ at 3.5-5 keV at 4-7°, with double beam modulation) to produce electron transparent cross-sectional specimens. Knowing the silicon wafer normal and by appropriate tilting of the silicon specimen in the transmission electron microscope (TEM), it was possible to ensure that the film was viewed edge-on.

2.4 Surface enhanced Raman scattering (SERS) measurements

In order to carry out surface enhanced Raman scattering (SERS) measurements, samples with PSZT thin films were rinsed with isopropyl alcohol, air-dried, and coated with silver. Silver thin films (thickness of 60 nm) were coated at normal incidence under rotation using an Emitech K975X thermal evaporator. The samples were then immersed for 10 minutes in the analyte (10 mM thiophenol diluted in ethanol), subsequently rinsed in pure ethanol, and air-dried. SERS measurements were carried out using a Jobin Yvon Horiba TRIAX320 spectrometer with a thermoelectrically cooled CCD detector. An objective lens of 50x, wavelength of 532 nm, and power of 1.1 mW were used. Data was collected in the backscatter mode with an acquisition time of 10 seconds.

2.5 Secondary ion mass spectrometry (SIMS) analysis

The SIMS analysis was carried out using caesium ions (Cs^+) with a primary accelerating voltage of 7.5 keV and a sampling voltage of 4.5 keV (Cameca 5f dynamic SIMS instrument). Considering the insulating nature of the film, the sample was biased with an offset voltage of +50 V to overcome charging effects. In view of the low concentration of strontium in the PSZT thin film samples, the two major isotopes - ^{86}Sr and ^{88}Sr - were studied to confirm the presence of strontium. The plotted data has been normalized with respect to the caesium signal measured.

2.6 X-ray diffraction (XRD) analysis

X-ray diffraction (XRD) analysis was carried out using a Scintag X-ray diffractometer operating with a cobalt X-ray source (at a wavelength of 0.179020 nm). The scans were carried out for a 2θ range of 20° to 60° with steps of 0.02°. The collected data were shifted to correspond to the copper $k\alpha$ wavelength (0.154056 nm) for comparison with the International Centre for Diffraction Data powder diffraction pattern files available.

3. Self-Assembled Island Structures

3.1 Island structured dielectric thin films

The deposition of platinum on silicon substrates typically requires the use of an intermediate adhesion layer. Inert titanium dioxide is commonly used in conjunction with pure silicon substrates (Pt/TiO₂/Si) (Bhaskaran et al., 2008), whereas titanium is the preferred layer for oxidized silicon surfaces (Pt/Ti/SiO₂/Si) (Kim et al., 1999; Million et al., 2003; Wasa et al., 2004). These two configurations prevent any reaction of the platinum with the silicon. However, in the synthesis process that we propose here, it is precisely this metal-silicon interaction which is the underlying mechanism.

Fabrication began by coating silicon substrates with a 20 nm titanium adhesion layer followed by 200 nm of platinum using electron beam evaporation. These samples were subsequently coated with dielectric thin films of strontium-doped lead zirconate titanate (PSZT) using RF magnetron sputtering.

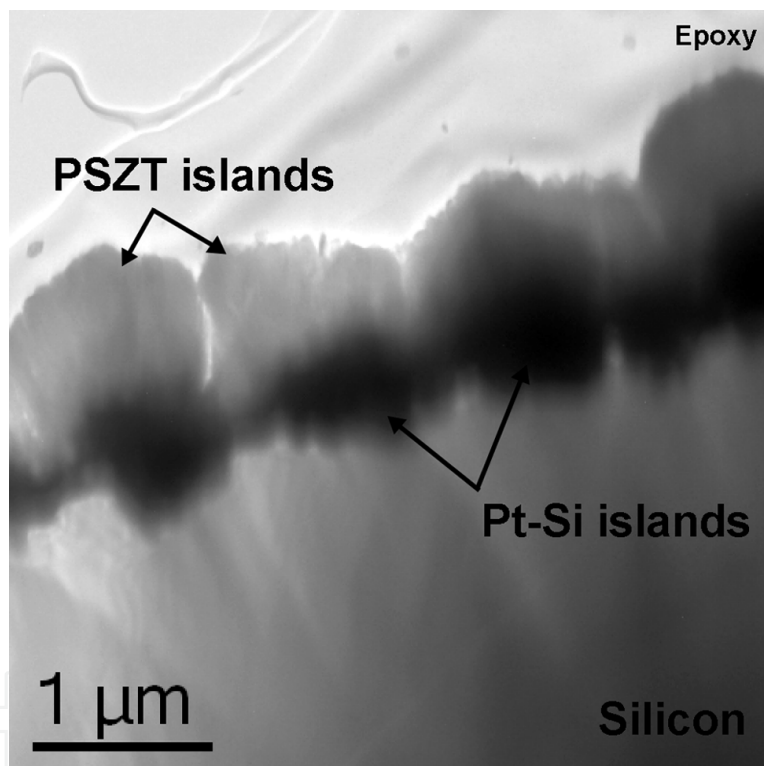


Fig. 1. Cross-sectional transmission electron micrograph analysis of PSZT thin films deposited on Pt/Ti/Si substrates. The distribution of Pt-Si islands and the preferential growth of PSZT on these islands can be observed. (Reprinted with permission from Sriram et al., 2009b)

The temperature of deposition initiates a reaction between the platinum and silicon through the thin titanium layer, resulting in the formation of islands of platinum silicide (Lee et al., 1997; Firebaugh et al., 1998). The PSZT thin film layer that is subsequently deposited prefers to grow on these platinum silicide islands. The affinity that PSZT-type films have for growing on metallic layers, and platinum in particular, has been established in the literature (Kim et al., 1999; Million et al., 2003; Wasa et al., 2004). The ability to form perovskite structured complex oxides on platinum has been used extensively for deposition processes. The platinum-silicon reaction and growth of sub-micron PSZT islands with columnar grains is shown in Fig. 1.

3.2 Mechanism of island structuring

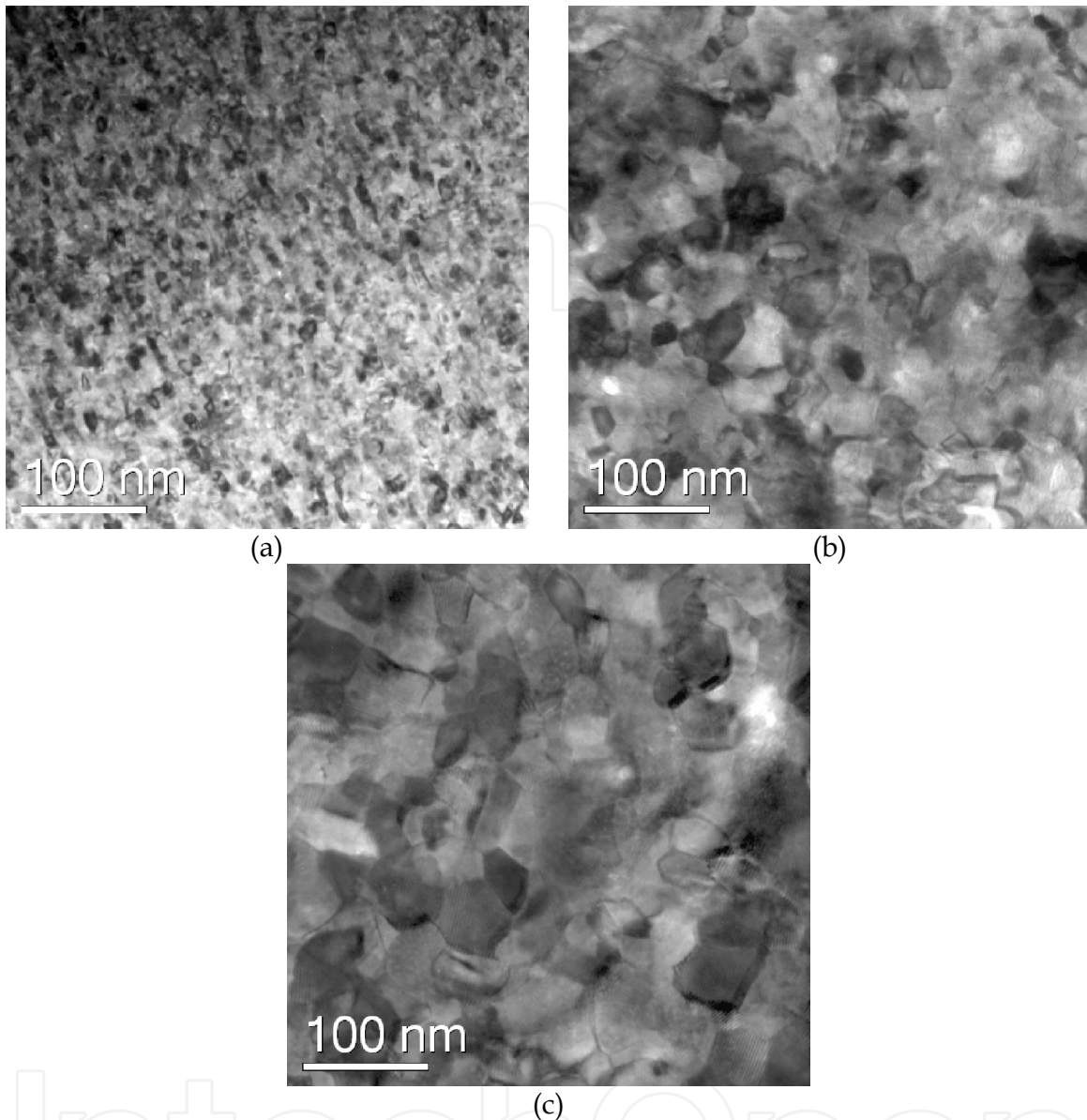


Fig. 2. TEM micrographs showing evolution of grains in the Pt/Ti/Si structure: (a) as-deposited sample, (b) at 500 °C, and (c) at 650 °C. (Reprinted with permission from Sriram et al., 2009b)

The mechanism responsible for the formation of the platinum-silicon islands was investigated using *in situ* heating during plan-view transmission electron microscopy (TEM) analysis. Silicon substrates coated with a 20 nm titanium adhesion layer and 200 nm of platinum were used. These samples were mechanically polished to create plan view TEM specimens. The samples were heated while being observed within the TEM to replicate the temperature ramp-up before the PSZT sputtering process.

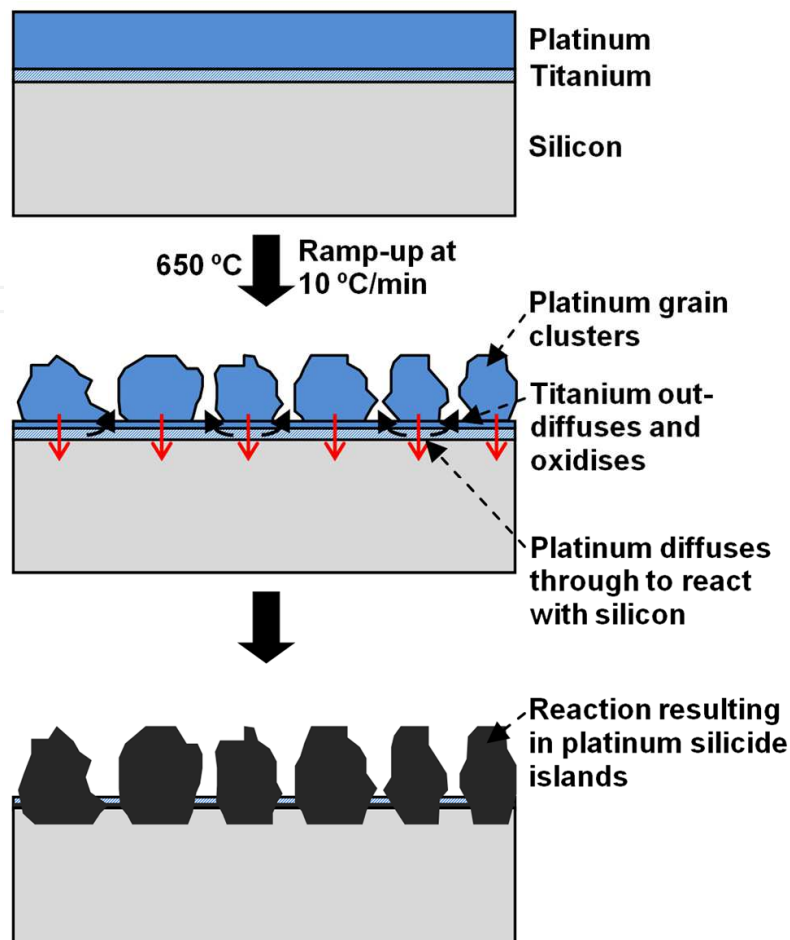


Fig. 3. Schematic depicting proposed mechanism for platinum-silicon reaction, based on *in situ* plan view TEM analysis, cross-section TEM analysis, and AES. (Reprinted with permission from Sriram et al., 2009b)

The evolution of the grain structure of platinum was studied by observing a region of the foil where the platinum layer overlapped with the silicon substrate. Grain growth with crystallization was apparent in the micrographs (Fig. 2), wherein an initial grain size of ~10 nm in the as-deposited sample increased to ~30 nm at 500 °C and ~50 nm at 650 °C. The distribution of grain sizes became more random with increasing temperature. Lattice fringes due to strong crystallization could be observed within individual grains. In the thinner regions of the specimen the formation of voids was observed, due to the formation of grain clusters. Each cluster consisted of 15-25 grains. The size and distribution of the clusters relate to the platinum-silicon islands observed in the cross-sectional micrographs (Fig. 1).

The composition of the island regions was examined by performing energy dispersive X-ray analysis (EDX), on the cross-section specimens. This analysis revealed that the island regions were composed of both platinum and silicon, while the regions between the islands had an upper surface that was rich in titanium and oxygen and a lower region composed mostly of platinum and silicon.

A possible explanation is as follows. As grain growth in platinum is initiated, outward diffusion of titanium occurs at the grain boundaries. This titanium is exposed to oxygen in the sputtering gas mixture and forms a stable oxide of titanium. As temperature increases,

platinum reacts with silicon to form islands of silicide, with regions of titanium oxide present in between. This oxide presumably prevents the formation of titanium silicide; and it is notable that stable titanium silicide is formed at temperatures above 700 °C (Maex & van Rossum, 1995; Bhaskaran et al., 2007). The presence of all four elements Si, Pt, Ti, and O was confirmed by using Auger electron spectroscopy (AES), while AES depth profiling verifies the existence of Pt-Si and surface Ti-O phases (Sriram et al., 2009b). A schematic depiction of the proposed mechanism is shown in Fig. 3.

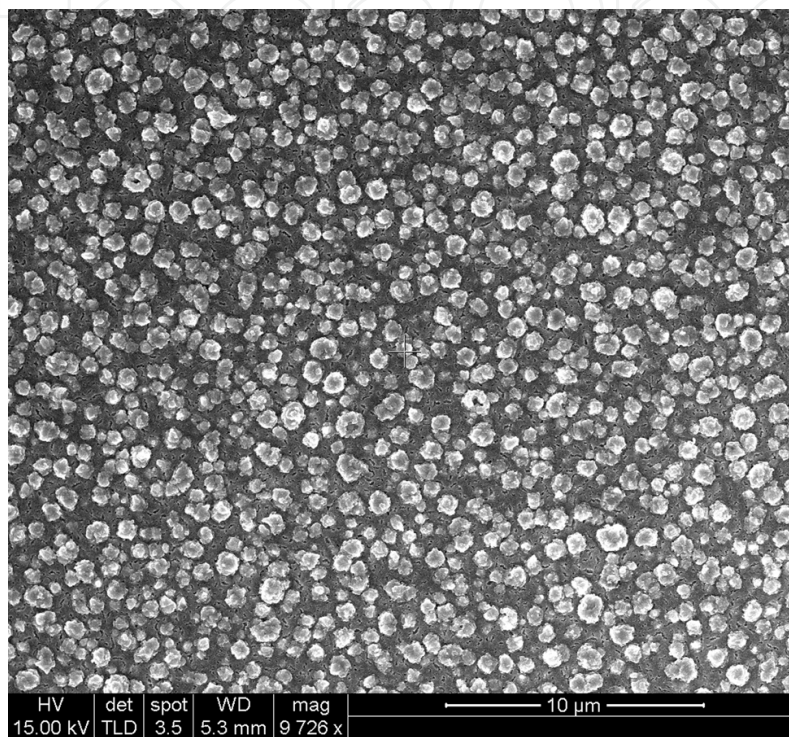


Fig. 4. Scanning electron micrograph depicting the distribution of the self-assembled Pt-Si islands with preferentially grown PSZT. (Reprinted with permission from Sriram et al., 2009b)

During the subsequent deposition of PSZT, it appears to preferentially grow on the regions with platinum, resulting in the final island-structure observed in the film, as shown in Fig. 1. The distribution and size of the islands depends on two factors that can be identified intuitively. These are the duration of thermal processing and the thickness of the platinum layer. The dependence on thermal processing duration was verified using cross-sectional TEM analysis, which showed that the average island size increased from ~500 nm for a 2 hour process to ~800 nm for a 4 hour process. The distribution of such islands on the substrate is shown in Fig. 4.

This island-structuring significantly increases the surface roughness of the samples under study. Analysis of average surface roughness (R_a) was carried out using an Ambios XP-2 surface profilometer. The Pt-Ti-Si electrode regions had a measured R_a of 24.8 nm and regions with PSZT deposited on them had R_a of 27.1 nm. This represents a significant increase over the R_a values for the continuous PSZT thin films on Pt/TiO₂/Si structure of 4.9 nm, with these electrodes registering an average surface roughness lesser than 2.0 nm.

3.3 Surface-enhanced Raman scattering results

The self-assembly of island features on a substrate and their subsequent transfer to thin films can be used effectively in a wide range of sensing applications. In this section, we demonstrate that the island structures that we have synthesized in both platinum and PSZT, have potential for applications in surface-enhanced Raman scattering (SERS) sensors.

SERS is a vibrational spectroscopy technique that allows sensitive detection of chemical compounds in close proximity to a nanostructured gold, silver or copper surface (Smith, 2008). The scattering efficiency can be enhanced by a factor of 10^6 or more compared to normal Raman scattering. The effect is primarily generated by the enhanced electromagnetic field associated with the localized surface plasmon resonance that occurs around the metal nanoparticles (Schatz et al., 2006; Stewart et al., 2008). The SERS effect can most readily be generated on roughened metal surfaces, where the roughness has a characteristic scale of 10-100 nm. Examples of such substrates include electrochemically roughened electrodes (Fleischmann et al., 1974; Pettinger & Wetzell, 1982) and metal films over nanoparticles (Goudonnet et al., 1982; Kostrewa et al., 1998). As a first step towards exploiting nanostructured dielectric films for plasmonic sensors, we have used the island-structured PSZT films as a platform for fabricating silver SERS substrates.

Four substrate types were employed for these SERS experiments. These were (i) continuous platinum thin film on silicon (Pt/TiO₂/Si), (ii) continuous PSZT thin film deposited on continuous platinum thin films (PSZT/Pt/TiO₂/Si), (iii) self-assembled Pt-Si islands, starting from the Pt/Ti/Si substrates and (iv) island-structured PSZT grown preferentially on the islands of substrates of type (iii).

The thicknesses of these layers were 200nm/20nm for Pt/TiO₂ on silicon substrate, while the PSZT dielectric layers were 750-800 nm, coated under the same conditions used for the island-structuring process. All four substrates were coated with a thin layer of silver to enable surface plasmonic activity. Thiophenol was used as the reference analyte, as it is widely used for SERS validation (Sandroff & Herschbach, 1982; Viets & Hill, 1998; Haynes et al., 2005; White & Stoddart, 2005; Kostovski et al., 2009).

The SERS spectra that were collected from the continuous platinum film substrates presented very weak spectral characteristics for thiophenol [Fig. 5(a)]. The peaks expected at $\sim 1000\text{ cm}^{-1}$, $\sim 1080\text{ cm}^{-1}$, and $\sim 1580\text{ cm}^{-1}$ could barely be resolved. Samples with the continuous PSZT layer [Fig. 5(b)] showed marginally better performance, albeit still unusable for SERS measurements.

SERS measurements for the island-structured substrates are shown in Figs. 5(c,d). Strong spectral signatures are present for the reference thiophenol peaks. A comparison of the intensities for the platinized substrates highlights that island-structuring [Fig. 5(c)] results in a 40x enhancement of Raman scattering over the continuous counterpart [Fig. 5(a)]. The inclusion of the PSZT layer [Fig. 5(d)] further enhances scattering counts by a factor of $2^{1/2}$. This represents a net 100x enhancement from the continuous metalized substrates to the island-structured PSZT substrates.

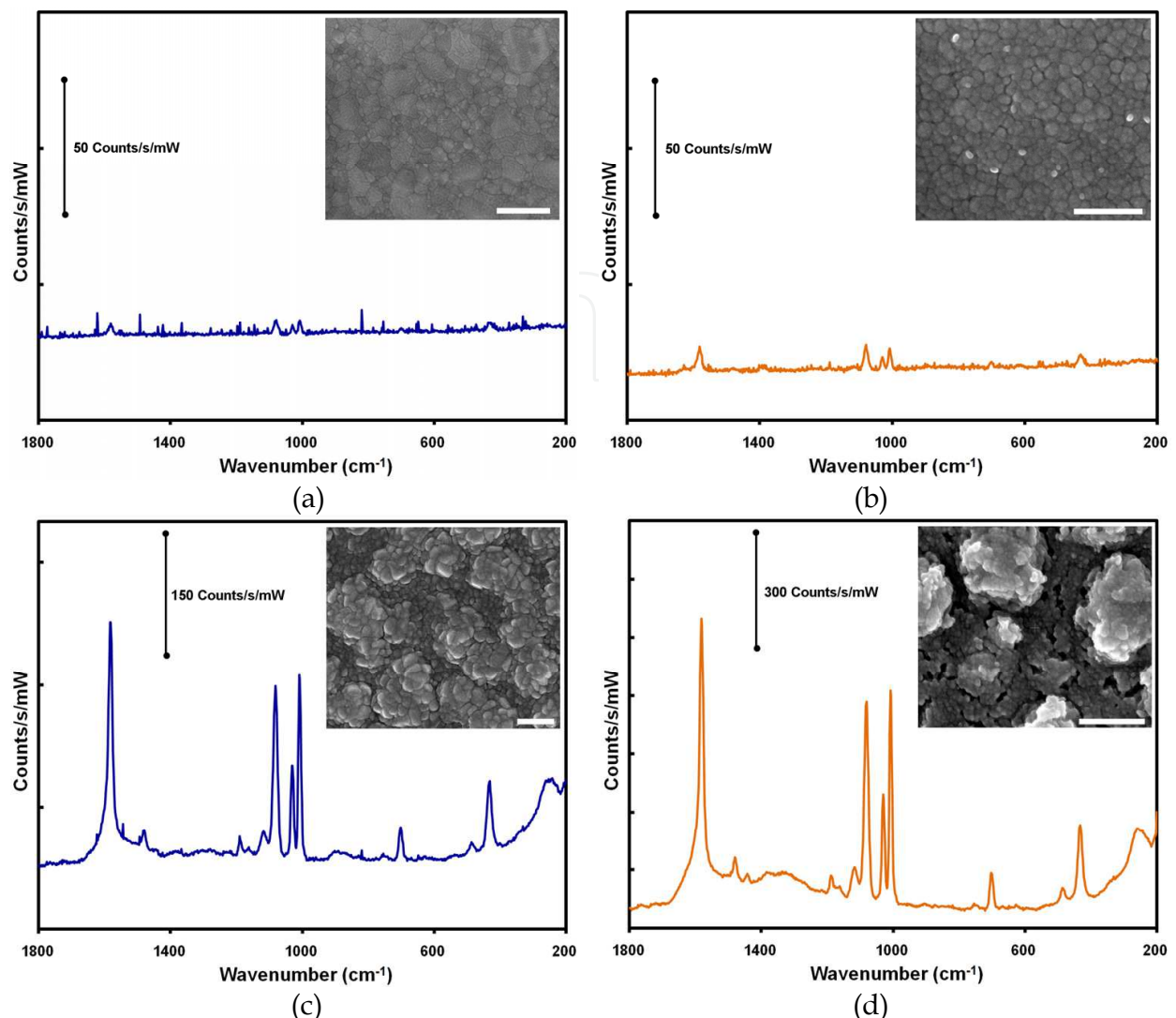


Fig. 5. SERS spectra collected for 10 mM thiophenol diluted in ethanol are presented. Spectra shown are for: (a) continuous platinum thin film on silicon; (b) continuous PSZT thin film deposited on substrate in (a); (c) self-assembled Pt-Si islands; and (d) island-structured PSZT grown preferentially on islands in (c). The interval between the y-axis markers is 50 counts/s/mW in (a) and (b) and is 150 counts/s/mW in (c) and (d). Scanning electron micrographs of the respective film surfaces coated with 60 nm of silver are shown as insets, with scale bars corresponding to 500 nm. (Reprinted with permission from Sriram et al., 2009b)

4. Low Temperature Deposition on Gold

4.1 PSZT thin films on Au/Ti/Si

Having chosen gold for having lattice spacings close to those of PSZT, thin films deposited on gold coated silicon substrates, with a titanium adhesion layer, were characterised. Secondary ion mass spectrometry (SIMS) depth profiling through the film thickness (Fig. 6) showed that it was compositionally uniform. The SIMS data also highlighted some dissolution of the titanium into the gold layer, although the peak in the titanium signal corresponded to the location of the original titanium layer (between the gold layer and the

silicon substrate). This depth profile was used to explain the results of certain observations during the transmission electron microscopy analysis. Figure 7 shows a low magnification cross-sectional view of the multi-layer structure. Energy dispersive X-ray analysis (EDX) was carried out along the length and through the thickness of the film to detect gross variations in chemical composition due to second phases or other contaminants; none were found. The PSZT film was uniform in thickness (~470 nm). The dark band beneath the film is the gold-titanium-silicon layer (typically ~135 nm thick), from which prismatic ingrowths into the silicon substrate can be seen.

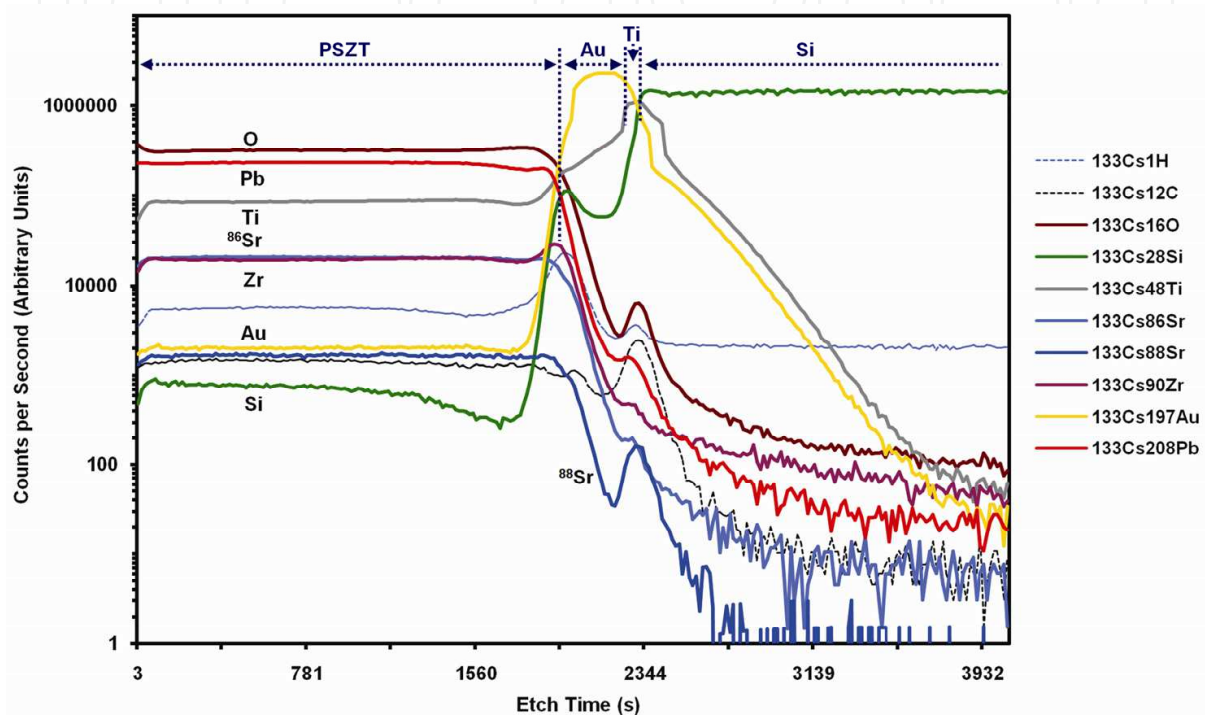


Fig. 6. Secondary ion mass spectroscopy depth profile through the thin film. (Reprinted with permission from Sriram et al., 2009c)

Detailed imaging of this interfacial region (Fig. 8) showed an amorphous layer approximately 4 nm thick. Point analysis with EDX showed that this layer was rich in silicon and oxygen, most likely SiO_2 formed by outward diffusion of silicon from the substrate through the metal layers. This is supported by previous studies on the fast outward diffusion of silicon through grain boundaries in gold (Sumida and Ikeda, 1991), with this silicon oxidising in the 10 % oxygen in argon sputtering atmosphere. This is also supported by the increase in the silicon signal at this interface in the SIMS analysis (also confirming that this is not a by-product of the specimen preparation ion milling process). The region of PSZT (~25 nm) closest to this amorphous SiO_2 layer appeared to be amorphous or at best poorly crystalline, as it exhibited strong amorphous speckle (right inset of Fig. 8). Weak lattice fringe contrast was only evident only from regions greater than 30 nm into the PSZT layer (from the SiO_2 interfacial layer, as seen in the left inset of Fig. 8).

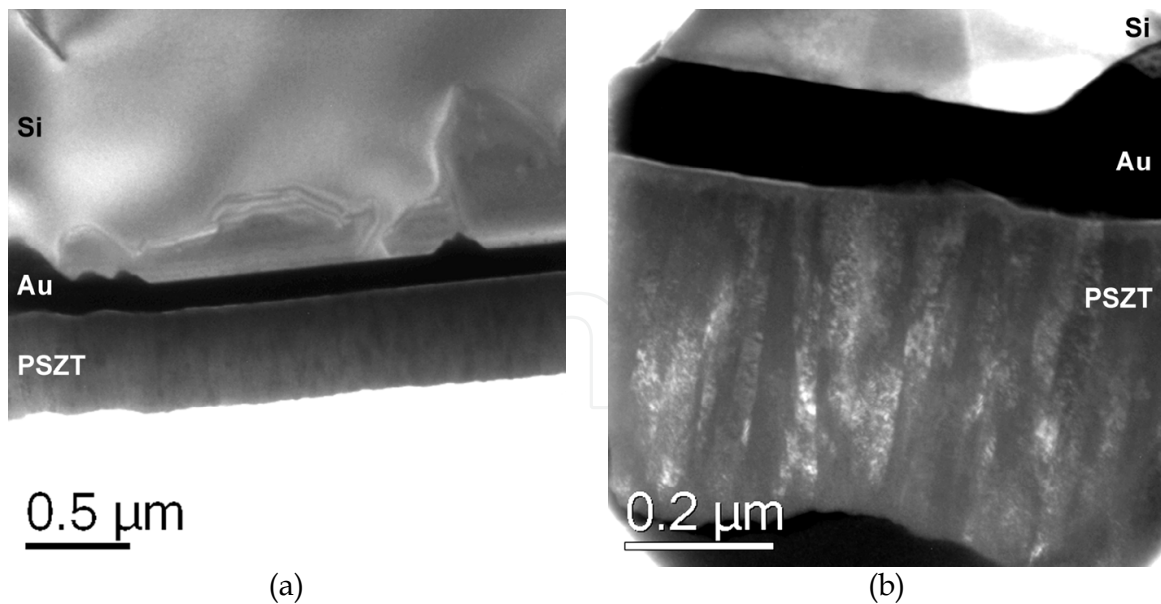


Fig. 7. XTEM analyses of a PSZT thin film deposited for a 2 hour sputtering duration: (a) Bright field diffraction contrast image of the ~470 nm thick PSZT film on a ~130 nm thick gold layer. Prismatic ingrowths of gold-silicon have formed at the interface of gold to silicon; (b) HCDF image of the PSZT film highlighting the columnar structure. *Note:* The outer region (~100 nm) of the film has been removed during ion-milling. (Reprinted with permission from Sriram et al., 2009c)

The PSZT thin film exhibited a columnar microstructure (Fig. 7). These columnar grains were perpendicular to the substrate (out of plane), and were most apparent in the energy filtered (zero loss) hollow cone dark field (HCDF) image [of a 2 hour PSZT deposition sample shown in Fig. 7(b)]. Typical columnar grain widths were 30-50 nm, and many grains appeared to span the full thickness of the film (~470 nm). The contrast due to the crystallinity was quite weak in the 25 nm thick band of PSZT closest to the gold layer, confirming the amorphous or poorly crystalline nature of this region (as observed in Fig. 8). During the initial stages of deposition, the PSZT is deposited onto a substrate covered with amorphous SiO₂, which affected crystallinity. Crystallisation of the PSZT occurs once a certain thickness of material (~25 nm) has been deposited. Growth stress may contribute to the onset of crystallisation (Mitchell et al., 2003). X-ray diffraction analysis of these films showed that the films exhibited preferential [104] orientation (discussed later).

Increasing the deposition duration from 2 to 4 hours increased the columnar grain width (measured from hollow cone dark field images) from 30-50 nm to ~90 nm (not shown). It also resulted in an increase in the average surface roughness (R_a) from 7.8 nm to 9.5 nm (Sriram et al., 2006b and Sriram et al., 2007). This was attributed to the development of marked faceting. Fig. 7(a) shows a cross-section of the relatively flat surface of the film deposited for 2 hours. The dimension of the weak faceting is similar to that of the columnar grain width (30-50 nm). For the film deposited for 4 hours, very pronounced prismatic faceting has occurred (Fig. 9). This is much coarser than seen at the shorter duration and reflects the grain coarsening taking place in the film in longer duration depositions. The increase in roughness is a consequence of grain coarsening, which can be attributed to the variations in growth rates as a function of crystal orientation as well as grain coalescence. At the growing surface, those grains in orientations promoting faster growth can dominate

neighbouring grains and eventually isolate them. With continued growth, grains may then develop prismatic faceting which causes increased surface roughening as the grain width increases (Mitchell et al., 2003).

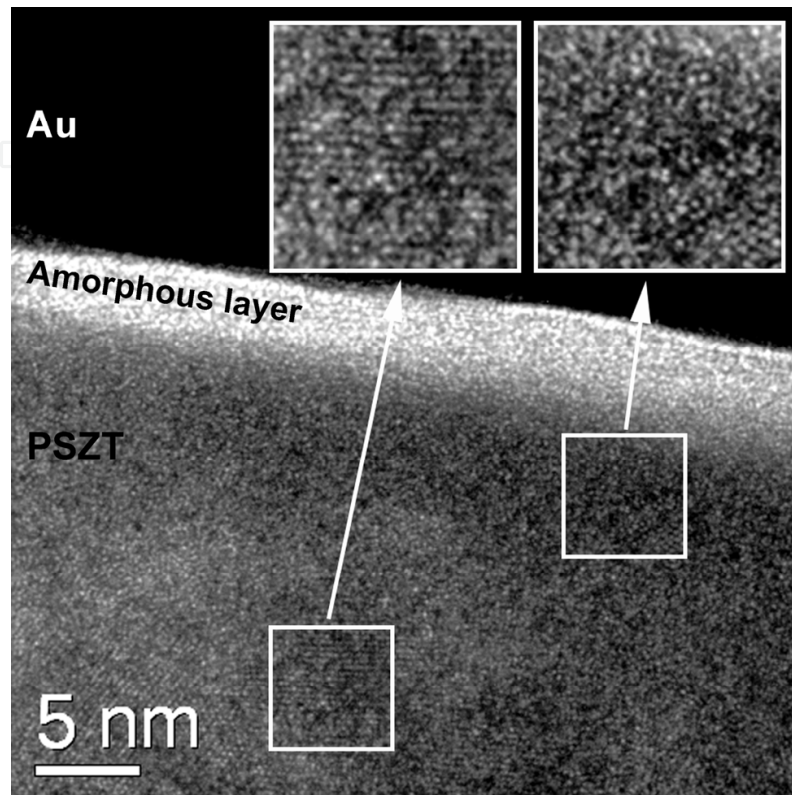


Fig. 8. High resolution energy filtered cross-sectional TEM image of the amorphous layer at the interface of PSZT and gold. (Reprinted with permission from Sriram et al., 2009c)

The eutectic point of gold and silicon is 363 °C, but at the deposition temperature of 300 °C interdiffusion of gold and silicon (enabled by outward silicon diffusion through gold grain boundaries) through the 15 nm thin titanium adhesion layer has been observed. This reaction was verified using secondary ion mass spectroscopy (SIMS) depth profiling (Fig. 6). The peak titanium concentration occurred between the gold and silicon - being the original location of the ~15 nm thick titanium layer. On moving through the gold layer towards the PSZT (a distance of 150 nm), the titanium signal showed a gradual decrease. This indicated that titanium diffused into the gold. Both titanium and gold diffusion into silicon was also apparent. The profiles for these two elements were very similar and gradually decreased over a considerable distance into the silicon. Due to the very different sputtering rates of the various phases present, it was not possible to meaningfully estimate the depth over which the gold and titanium diffused into the silicon substrate. However, the cross-sectional TEM imaging provided an understanding of the origin of the SIMS profile shapes for these elements.

The gold-(titanium)-silicon reaction can be observed in the form of prismatic crystallites growing into silicon along the metal-silicon interface. This is shown in Figs. 7 and 9 and in detail in Fig. 10. EDX analysis confirmed that these crystallites were a reaction product of gold and silicon - with titanium also present (Sriram et al., 2009c). The remnant of the

original titanium layer could be seen as a ~10 nm wide band running across the base of the crystallite in Fig. 10. The crystallites were variable in size, the largest being about 200 nm into silicon. During SIMS depth profiling (Fig. 6), the floor of the ion milling crater would break through the main (flat) part of the metal layer into the silicon substrate, and the gold and titanium signals would be expected to drop abruptly. However, the presence of prismatic crystallites rich in gold, with traces of titanium, projecting into the silicon substrate, would cause the signal for these elements to taper off gradually as the depth profiling progressed, dropping to zero when the profile passed through the apex of the largest crystallites.

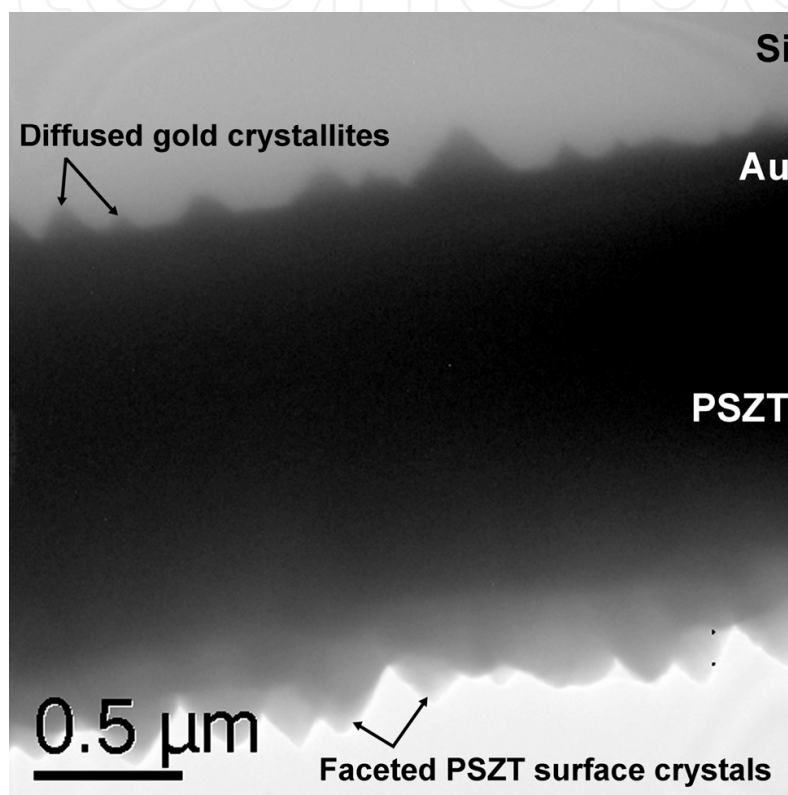


Fig. 9. Cross-section energy filtered TEM image showing the highly faceted film surface with crystallites at the gold-silicon interface. (Reprinted with permission from Sriram et al., 2009c)

The diffusion of gold into the (100) silicon results in crystallites bounded by the dense (111) silicon planes (Fig. 10). As expected the angle between these bounding planes and the silicon (100) surface was found to be 54.7° in Fig. 10, which is oriented with the electron beam parallel to silicon [110]. The resulting crystallites varied in size and the density of such crystallites was much higher in longer duration deposition (4 h) specimen. Such diffusion or dissolution of gold into silicon-based materials through titanium has been observed (Wenzel et al., 1998) and can be related to the high reactivity of titanium with silicon (Ti_xSi_y compounds are formed even at slightly elevated temperatures) and the thickness (15 nm) of the titanium layer. It has also been concluded that the titanium layer needs to have a sufficient thickness, depending on process temperature and duration, in order to serve as a barrier to prevent the gold-silicon reaction (Kanamori and Sudo, 1982), rather than serve only as an adhesion layer.

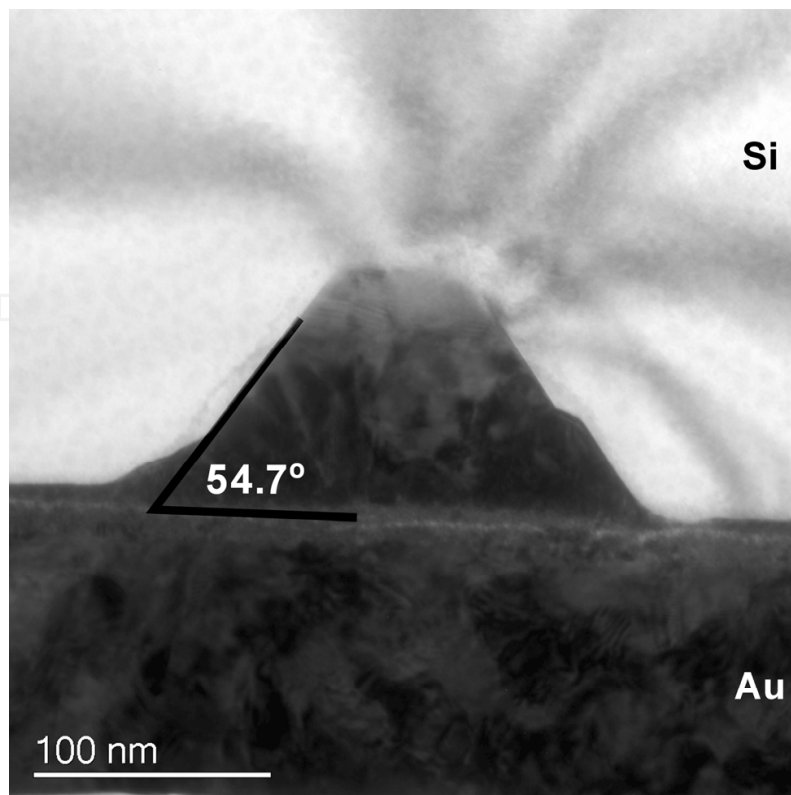


Fig. 10. Cross-sectional energy filtered TEM image of a crystallite bounded by dense (111) silicon planes. The angle between the silicon (100) surface and the crystallite edge is 54.7° being the silicon (100)^{^(111)} interplanar angle. *Note:* The electron beam is parallel to silicon [110]. (Reprinted with permission from Sriram et al., 2009c)

4.2 PSZT thin films on Au/Ti/SiO₂/Si

To overcome the gold-silicon interdiffusion observed in the initial samples, an intermediate silicon dioxide (SiO₂, 200 nm thick) layer was introduced between the metal layers and silicon, and PSZT deposition was carried out at 300 °C. The silicon dioxide layer included between the metal layers and the silicon substrate prevents metal-silicon reactions, and uniform thin film layers can be observed in the cross-sectional transmission electron micrograph [Fig. 11(a)]. The resulting PSZT films had a nanocolumnar grain structure. The PSZT deposition temperature initiates crystal growth in the gold layer (which was nanocrystalline when deposited), resulting in significant changes to the texture of gold [Fig. 11(b)]. In the absence of gold-silicon interactions, the gold layer is able to reorient so that the most densely packed planes (111) are parallel to the surface, and thus the surface energy is minimized. The formation of the amorphous layer is also prevented. As a result, the highly textured gold layer was able exert a strong guiding effect on the subsequently deposited PSZT thin films (Fig. 12), which developed a pronounced (104) texture (discussed later). This guiding effect results in the (104) PSZT planes being aligned parallel to (111) gold planes (Fig. 13); this is a feature at different points along the interface interspersed with regions of random orientation.

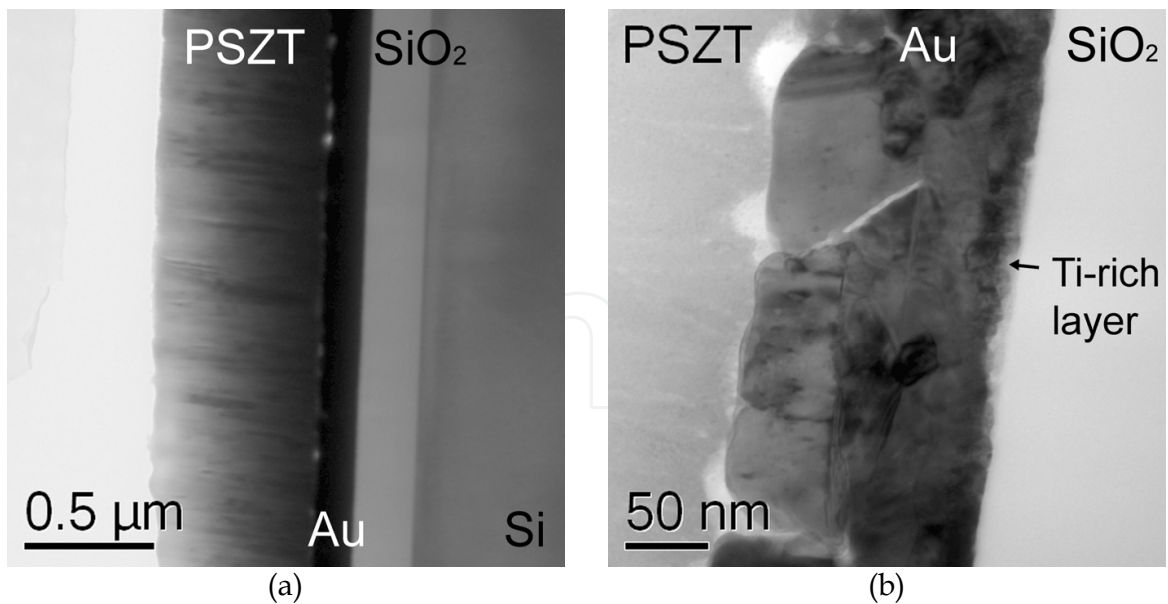


Fig. 11. Cross-sectional transmission electron microscopy results: (a) uniform thin film layers can be observed in the cross-sectional transmission electron micrograph and (b) grain growth in gold with preferential (111) texturing (lattice spacing of 0.236 nm). (Reprinted with permission from Sriram et al., 2010)

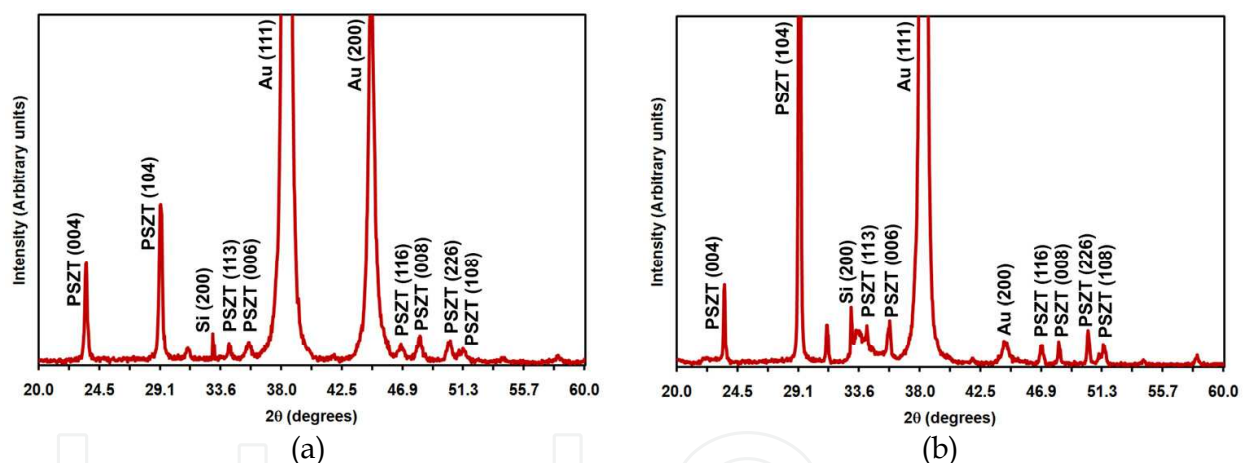


Fig. 12. X-ray diffraction results indicating preferential orientation in the gold and PSZT layers: (a) PSZT on Au/Ti/Si and (b) PSZT on Au/Ti/SiO₂/Si. (Reprinted with permission from Sriram et al., 2010)

The ratio of the relative intensities of the (111) and (200) gold X-ray diffraction peaks was ~100 after PSZT deposition at 300 °C on a sample with the buffer layer of silicon dioxide [Fig. 12(b)]; this corresponds to an increase in preferential orientation in the gold layer by a factor of 6 (compared to a sample without the silicon dioxide layer) [Fig. 12(a)].

The pronounced (111) orientation in the gold layer improves the preferential orientation of the PSZT thin film - the ratio of the X-ray diffraction relative intensities of the two major peaks corresponding to (004) and (104) PSZT orientations increased from 1.57 to 8.52 with the inclusion of the silicon dioxide layer (Fig. 12). All PSZT thin film peaks were shifted from expected peak positions, while substrate (gold and silicon) peaks were exactly at expected peak positions. The PSZT rhombohedral unit cell parameters *a* and *c* were both about 5.29%

larger than expected. This diffraction analysis also showed that the unit cells of the PSZT thin films have a 16% greater volume than theoretically expected (Bhaskaran et al., 2008).

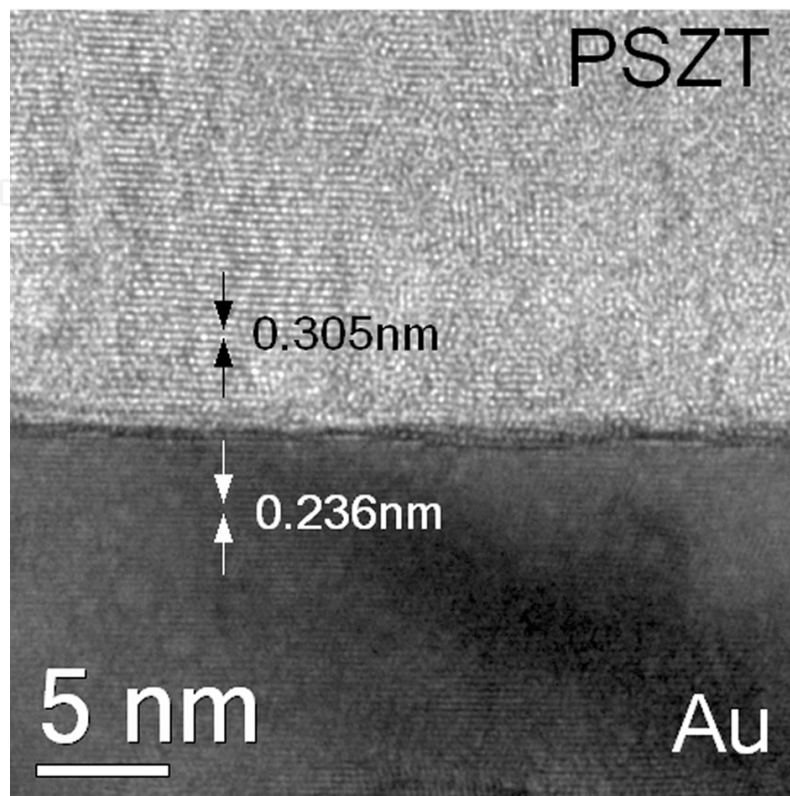


Fig. 13. The preferentially oriented gold layer appears to have a guiding effect on the PSZT thin film and this high resolution transmission electron micrograph shows the (104) planes of PSZT (with lattice spacing of 0.305 nm) preferentially aligning parallel to the (111) gold planes. (Reprinted with permission from Sriram et al., 2010)

Crystal structure simulations carried out using these modified unit cell parameters highlight the small lattice mismatches between the gold (111) and PSZT (104) planes as depicted in Fig. 14. From the overlap of atoms of these planes it can be concluded that gold can exert a guiding effect on PSZT. The simulation for gold was based on a lattice constant a of 0.236 nm and that for PSZT was based on the modified rhombohedral unit cell parameters a of 0.604 nm and c of 1.508 nm.

Based on the lattice spacing parameters (Sriram et al., 2010), a guiding effect by gold (111) on PSZT (202) might have been expected. According to the powder diffraction reference,[§] the PSZT (104) is five times more intense than the (202) orientation, indicating that the former is the preferred equilibrium state. This is the most likely reason for the observed guiding effect of gold (111) on PSZT (104). It should also be noted that the proximity of the d -spacings of the gold (111) and PSZT (202) peaks thwarts structural comparison using XRD, with no related guiding effects observed in the XTEM results. Importantly, the crystal structure simulations presented in Fig. 14 verifies the atomic overlap and the ability of gold (111) to exert a guiding effect on PSZT (104).

[§] Powder Diffraction Pattern Files, International Centre for Diffraction Data (ICDD, formerly the Joint Committee for Powder Diffraction Studies), Newtown Square, PA 19073, Card 04-002-5985.

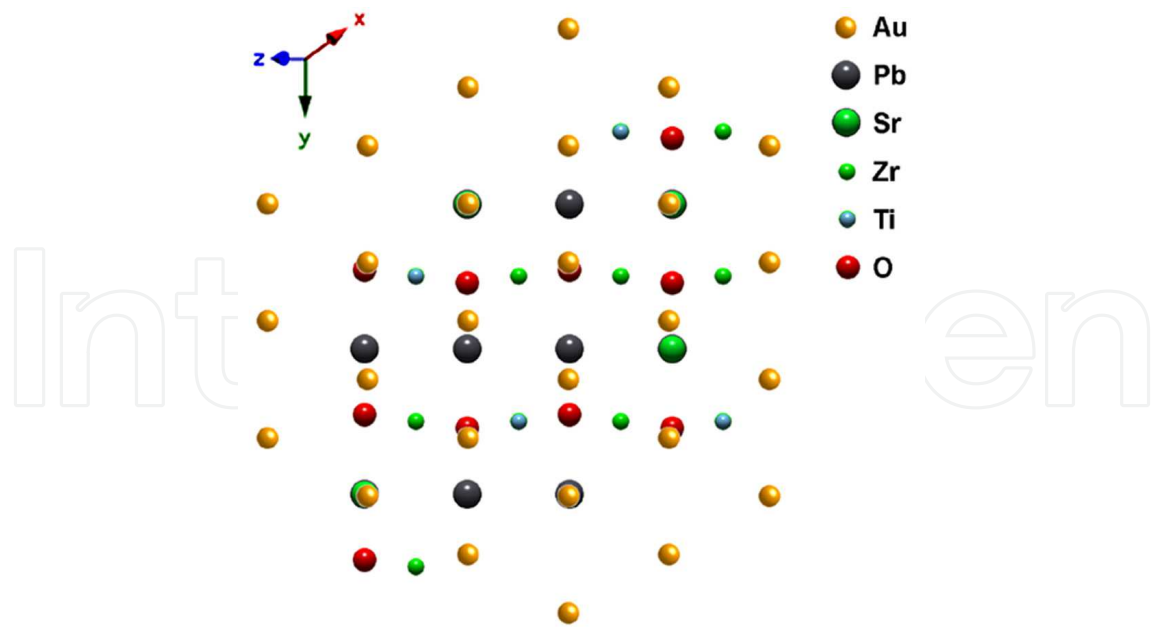


Fig. 14. Crystal structure simulation showing the superposition of the gold (111) plane on the PSZT (104) plane. From the overlap of atoms of these planes it can be concluded that gold can exert a guiding effect on PSZT. (Reprinted with permission from Sriram et al., 2010)

5. Conclusion

Extensive materials characterisation of PSZT thin films deposited on platinum and gold coated silicon substrates has been performed. The focus has been on silicon substrate based studies, in order to enable future incorporation of PSZT thin films in silicon-based devices. Spectroscopy and microscopy techniques were used, often in combination, to study the microstructure of the deposited thin films.

A synthesis process for realizing island-structured textures was proposed by inciting a reaction between the silicon substrate and the platinum thin film layer deposited on it. This process results in a distribution of sub-micron and nanoscale islands of platinum silicide, with the process scalability dependent on thermal duration and metal thickness parameters. A mechanism for this structuring process is proposed, combining results from microscopy and spectroscopy analyses. The ability of these textures to serve as SERS-active media is demonstrated, with 100x enhancement of detection sensitivity demonstrated for thiophenol as compared to the planar substrates. Further enhancement of the SERS sensitivity could be expected by optimising the silicide island morphology through control of the annealing conditions and through engineering of the nano-scale column structure of the complex oxide to best accommodate a specific analyte.

A combination of transmission electron microscopy and X-ray diffraction has been used to show that gold exerts a guiding effect on the RF magnetron sputter deposited PSZT thin films. PSZT thin films deposited on gold-coated silicon substrates using titanium as an adhesion layer showed presence of inter-diffusion. PSZT films exhibited a uniform composition through their thickness. A silicon-rich amorphous layer was formed at the interface of the PSZT thin films and gold, and was most likely to be silicon dioxide. Prismatic crystallites of a gold-silicon compound developed at the interface of the metal layers and the silicon substrate. This was caused by gold diffusing through the underlying

titanium metal layer; the crystallites being bounded by the dense (111) silicon planes. On the introduction of a silicon dioxide barrier layer, the resulting films have a nanocolumnar grain structure with strong preferential orientation. This is one of the first instances of low temperature deposition of preferentially oriented piezoelectric thin films, with this deposition on silicon making the process favourable to microfabrication processes. This has the potential for enabling incorporation of complex functional oxides into devices with processing at a relatively lower temperature of 300 °C, allowing more versatile device designs and fabrication schemes. The guiding effect of (111) Au on (104) PSZT was observed by high resolution transmission electron microscopy and verified using crystal structure simulations.

These results pave the way for the next generation of high performance piezoelectric thin film devices on silicon.

Acknowledgements

The authors acknowledge funding support from the Australian Research Council (Discovery Project DP1092717) and the Australian Institute of Nuclear Science and Engineering. The authors also thank researchers who contributed to this work - A. S. Holland, G. Kostovski, D. R. G. Mitchell, K. T. Short, and P. R. Stoddart.

6. References

- Araujo, E. B. & Eiras, J. A. (2003). Effects of crystallization conditions on dielectric and ferroelectric properties of PZT thin films. *Journal of Physics D: Applied Physics*, 36, 16, 2010-2013, 0022-3727
- Bedoya, C.; Muller, C.; Baudour, J.-L.; Madigou, V.; Anne, M. & Roubin, M. (2000). Sr-doped $\text{PbZr}_{1-x}\text{Ti}_x\text{O}_3$ ceramic: Structural study and field-induced reorientation of ferroelectric domains. *Materials Science Engineering B*, 75, 1, 43-52, 0921-5107
- Bhaskaran, M.; Sriram, S.; Short, K. T.; Mitchell, D. R. G.; Holland, A. S. & Reeves, G. K. (2007). Characterisation of C54 titanium silicide thin films by spectroscopy, microscopy and diffraction. *Journal of Physics D: Applied Physics*, 40, 17, 5213-5219, 0022-3727
- Bhaskaran, M.; Sriram, S.; Mitchell, D. R. G.; Short, K. T. & Holland, A. S. (2008). Effect of multi-layered bottom electrodes on the orientation of strontium-doped lead zirconate titanate thin films. *Thin Solid Films*, 516, 22, 8101-8105, 0040-6090
- Firebaugh, S. L.; Jensen, K. F. & Schmidt, M. A. (1998). Investigation of high-temperature degradation of platinum thin films with an in situ resistance measurement apparatus. *Journal of Microelectromechanical Systems*, 7, 1, 128-135, 1057-7157
- Fleischmann, M.; Hendra, P. J. & McQuillan, A. J. (1974). Raman spectra of pyridine adsorbed at a silver electrode. *Chemical Physics Letters*, 26, 2, 163-166, 0009-2614
- Goudonnet, J. P.; Begun, G. M. & Arakawa, E. T. (1982). Surface-enhanced raman scattering on silver-coated teflon sphere substrates. *Chemical Physics Letters*, 92, 2, 197-201, 0009-2614

- Haynes, C. L.; Yonzon, C. R.; Zhang, X. & Van Duyne, R. P. (2005). Surface-enhanced Raman sensors: early history and the development of sensors for quantitative biowarfare agent and glucose detection. *Journal of Raman Spectroscopy*, 36, 6-7, 471-484, 0377-0486
- Kanamori, S. & Sudo, H. (1982). Effects of titanium layer as diffusion barrier in Ti/Pt/Au beam lead metallization on polysilicon. *IEEE Transactions on Components Hybrids and Manufacturing Technology*, CHMT-5, 318-321, 0148-6411
- Kim, T. S.; Kim, D. J. & Jung, H. J. (1999). N₂O reactive gas effect on rf magnetron sputtered Pb(Zr_{0.52}Ti_{0.48})O₃ thin films. *Journal of Applied Physics*, 86, 7024-7028, 0021-8979
- Kostovski, G.; White, D. J.; Mitchell, A.; Austin, M. W. & Stoddart, P. R. (2009). Nanoimprinted optical fibres: Biotemplated nanostructures for SERS sensing. *Biosensors and Bioelectronics*, 24, 5, 1531-1535, 0956-5663
- Kostrewa, S.; Hill, W. & Klockow, D. (1998). Silver films on diamond particles as substrates for surface-enhanced Raman scattering. *Sensors and Actuators B: Chemical*, 51, 1-3, 292-297, 0925-4005
- Lee, C.-K.; Hsieh, C.-D. & Tseng, B.-H. (1997). Effects of a titanium interlayer on the formation of platinum silicides. *Thin Solid Films*, 303, 1-2, 232-237, 0040-6090
- Maex, K. & van Rossum, M. (1995). In: *Properties of Metal Silicides*, INSPEC, 0863417760, London
- Maluf, N. & Williams, K. (2004). *An Introduction to Microelectromechanical Systems Engineering*, Artech House, 9781580535915, Norwood
- Millon, C.; Malhaire, C.; Dubois, C. & Barbier, D. (2002). Control of the Ti diffusion in Pt/Ti bottom electrodes for the fabrication of PZT thin film transducers. *Materials Science in Semiconductor Processing*, 5, 2-3, 243-247, 1369-8001
- Mitchell, D. R. G.; Attard, D. J. & Triani, G. (2003). Transmission electron microscopy studies of atomic layer deposition TiO₂ films grown on silicon. *Thin Solid Films*, 441, 1-2, 85-95, 0040-6090
- Park, C.-S.; Kim, S.-W.; Park, G.-T.; Choi, J.-J. & Kim, H.-E. (2005b). Orientation control of lead zirconate titanate film by combination of sol-gel and sputtering deposition. *Journal of Materials Research*, 20, 1, 243-246, 0884-2914
- Park, J. H.; Kwon, T. Y.; Yoon, D. S.; Kim, H. & Kim, T. S. (2005a). Fabrication of microcantilever sensors actuated by piezoelectric Pb(Zr_{0.52}Ti_{0.48})O₃ thick films and determination of their electromechanical characteristics. *Advanced Functional Materials*, 15, 12, 2021-2028, 1616-3028
- Pettinger, B. & Wetzel, H. (1982). In: *Surface-Enhanced Raman Scattering*, Chang, R. K., Furtak, T. E., Eds.; 293, Plenum Press, 9780306409073, New York
- Randall, C. A.; Kim, N.; Kucera, J.-P.; Cao, W. & ShROUT, T. R. (1998). Intrinsic and extrinsic size effects in fine-grained morphotropic-phase-boundary lead zirconate titanate ceramics. *Journal of the American Ceramic Society*, 81, 3, 677-688, 0002-7820
- Sandhoff, C. J. & Herschbach, D. R. (1982). Surface-enhanced Raman study of organic sulfides adsorbed on silver: facile cleavage of sulfur-sulfur and carbon-sulfur bonds. *Journal of Physical Chemistry*, 86, 17, 3277-3279
- Schatz, G. C.; Young, M. A. & Van Duyne, R. P. (2006). In: *Surface-Enhanced Raman Scattering: Physics and Applications*, Kneipp, K., Moskovits, M., Kneipp, H., Eds.; 19-45, Springer-Verlag, 3540335668, Heidelberg

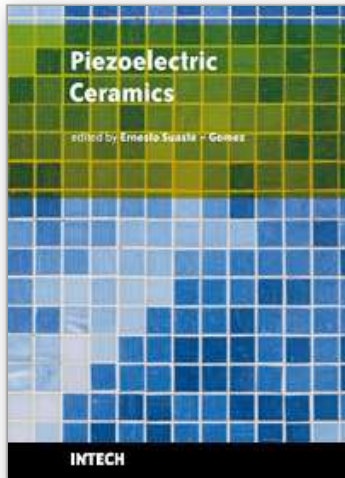
- Smith, W. E. (2008). Practical understanding and use of surface enhanced Raman scattering/surface enhanced resonance Raman scattering in chemical and biological analysis. *Chemical Society Reviews*, 37, 955-964, 0306-0012
- Sriram, S.; Bhaskaran, M. & Holland, A. S. (2006a). The effect of post-deposition cooling rate on the orientation of piezoelectric $(\text{Pb}_{0.92}\text{Sr}_{0.08})(\text{Zr}_{0.65}\text{Ti}_{0.35})\text{O}_3$ thin films deposited by RF magnetron sputtering. *Semiconductor Science and Technology*, 21, 9, 1236-1243, 0268-1242
- Sriram, S.; Bhaskaran, M. & Holland, A. S. (2006b). Surface morphology and stress analysis of piezoelectric strontium doped lead zirconate titanate thin films, *Proceedings of the SPIE (Micro- and Nanotechnology: Materials, Processes, Packaging, and Systems III)*, p. 64150J, 9780819465238, Adelaide, December 2006, SPIE, Bellingham
- Sriram, S.; Bhaskaran, M.; Holland, A. S.; Short, K. T. & Latella, B. A. (2007). Measurement of high piezoelectric response of strontium-doped lead zirconate titanate thin films using a nanoindenter. *Journal of Applied Physics*, 101, 104910, 0021-8979
- Sriram, S.; Bhaskaran, M.; du Plessis, J.; Short, K. T.; Sivan, V. P. & Holland, A. S. (2009a). Influence of oxygen partial pressure on the composition and orientation of strontium-doped lead zirconate titanate thin films. *Micron*, 40, 1, 104-108, 0968-4328
- Sriram, S.; Bhaskaran, M.; Kostovski, G.; Mitchell, D. R. G.; Stoddart, P. R.; Austin, M. W. & Mitchell, A. (2009b). Synthesis of Self-Assembled Island-Structured Complex Oxide Dielectric Films. *Journal of Physical Chemistry C*, 113, 38, 16610-16614, 1932-7447
- Sriram, S.; Bhaskaran, M.; Mitchell, D. R. G.; Short, K. T.; Holland, A. S. & Mitchell, A. (2009c). Microstructural and Compositional Analysis of Strontium-Doped Lead Zirconate Titanate Thin Films on Gold-Coated Silicon Substrates. *Microscopy and Microanalysis*, 15, 30-35, 1431-9276
- Sriram, S.; Bhaskaran, M.; Mitchell, D. R. G. & Mitchell, A. (2010). Lattice Guiding for Low Temperature Crystallization of Rhombohedral Perovskite-Structured Oxide Thin Films. *Crystal Growth & Design*, 10, 2, 761-764, 1528-7483
- Stewart, M. E.; Anderton, C. R.; Thompson, L. B.; Maria, J.; Gray, S. K.; Roger, J. A. & Nuzzo, R. G. (2008). Nanostructured Plasmonic Sensors. *Chemical Reviews*, 108, 2, 494-521, 1520-6890
- Sumida, N. & Ikeda, K. (1991). Cross-sectional observations of gold-silicon reaction on silicon substrate in situ in the highvoltage electron microscope. *Ultramicroscopy*, 39, 1-4, 313-320, 0304-3991
- Tunaboylu, B.; Harvey, P. & Esener, S. C. (1998). Microstructure of magnetron sputtered PLZT thin films on sapphire. *Integrated Ferroelectrics*, 19, 1-4, 11-32, 1058-4587
- Viets, C. & Hill, W. (1998). Comparison of fibre-optic SERS sensors with differently prepared tips. *Sensors and Actuators B: Chemical*, 51, 1, 92-99, 0925-4005
- Wasa, K.; Kitabatake, M. & Adachi, H. (2004). *Thin Film Materials Technology: Sputtering of Compound Materials*, Springer-Verlag, 9783540211181, Heidelberg
- Wenzel, R.; Goesmann, F. & Schmid-Fetzer, R. (1998). Diffusion barriers in gold-metallized titanium-based contact structures on SiC. *Journal of Materials Science: Materials in Electronics*, 9, 109-113, 0957-4522
- White, D. J. & Stoddart, P. R. (2005). Nanostructured optical fiber with surface-enhanced Raman scattering functionality. *Optics Letters*, 30, 6, 598-600, 0146-9592

- Yu, Y. & Singh, R. N. (2000). Effect of composition and temperature on field-induced properties in the lead strontium zirconate titanate system. *Journal of Applied Physics*, 88, 12, 7249-7257, 0021-8979
- Yu, Y.; Tu, J. & Singh, R. N. (2001). Phase stability and ferroelectric properties of lead strontium zirconate titanate ceramics. *Journal of the American Ceramic Society*, 84, 2, 333-340, 0002-7820
- Zheng, H.; Reaney, I. M.; Lee, W. E.; Jones, N. & Thomas, H. (2002). Surface decomposition of strontium-doped soft $\text{PbZrO}_3\text{-PbTiO}_3$. *Journal of the American Ceramic Society*, 85, 1, 207-212, 0002-7820

IntechOpen

IntechOpen

IntechOpen



Piezoelectric Ceramics

Edited by Ernesto Suaste-Gomez

ISBN 978-953-307-122-0

Hard cover, 294 pages

Publisher Sciyo

Published online 05, October, 2010

Published in print edition October, 2010

This book reviews a big window of opportunity for piezoelectric ceramics, such as new materials, material combinations, structures, damages and porosity effects. In addition, applications of sensors, actuators, transducers for ultrasonic imaging, positioning systems, energy harvesting, biomedical and microelectronic devices are described. The book consists of fourteen chapters. The genetic algorithm is used for identification of RLC parameters in the equivalent electrical circuit of piezoelectric transducers. Concept and development perspectives for piezoelectric energy harvesting are described. The characterization of principal properties and advantages of a novel device called ceramic-controlled piezoelectric with a Pt wire implant is included. Bio-compatibility studies between piezoelectric ceramic material and biological cell suspension are exposed. Thus, piezoelectric ceramics have been a very favorable solution as a consequence of its high energy density and the variety of fabrication techniques to obtain bulk or thin films devices. Finally, the readers will perceive a trend analysis and examine recent developments in different fields of applications of piezoelectric ceramics.

How to reference

In order to correctly reference this scholarly work, feel free to copy and paste the following:

Sharath Sriram, Madhu Bhaskaran and Arnan Mitchell (2010). Piezoelectric Thin Film Deposition: Novel Self-Assembled Island Structures and Low Temperature Processes on Silicon, Piezoelectric Ceramics, Ernesto Suaste-Gomez (Ed.), ISBN: 978-953-307-122-0, InTech, Available from:

<http://www.intechopen.com/books/piezoelectric-ceramics/piezoelectric-thin-film-deposition-novel-self-assembled-island-structures-and-low-temperature-proces>

INTECH
open science | open minds

InTech Europe

University Campus STeP Ri
Slavka Krautzeka 83/A
51000 Rijeka, Croatia
Phone: +385 (51) 770 447
Fax: +385 (51) 686 166
www.intechopen.com

InTech China

Unit 405, Office Block, Hotel Equatorial Shanghai
No.65, Yan An Road (West), Shanghai, 200040, China
中国上海市延安西路65号上海国际贵都大饭店办公楼405单元
Phone: +86-21-62489820
Fax: +86-21-62489821

© 2010 The Author(s). Licensee IntechOpen. This chapter is distributed under the terms of the [Creative Commons Attribution-NonCommercial-ShareAlike-3.0 License](#), which permits use, distribution and reproduction for non-commercial purposes, provided the original is properly cited and derivative works building on this content are distributed under the same license.

IntechOpen

IntechOpen